

Effects of SnO₂ layer coated on carbon nanofiber for the methanol oxidation reaction



Dong Ha Kim, Dong-Yo Shin, Young-Geun Lee, Geon-Hyoung An, Jeong Hwan Han, Hyo-Jin Ahn, Byung Joon Choi*

Department of Materials Science and Engineering, Seoul National University of Science and Technology, Seoul 01811, Republic of Korea

ARTICLE INFO

Keywords:

Coating materials
Nanostructured materials
Fuel cells
Vapor deposition
Electrochemical reactions

ABSTRACT

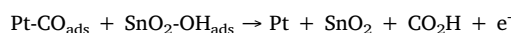
Carbon nanofibers (CNFs) are used as active materials for electrodes in various energy devices, such as lithium ion secondary batteries, supercapacitors, and fuel cells. Recent studies have shown that nanoscale coatings on carbon nanotubes increase the output and lifespan of these devices owing to the improvement of their mechanical and chemical properties. Among various coating methods, atomic layer deposition (ALD) can adjust the thickness of the coating layer conformally without any directional growth. Therefore, ALD can coat particles with high aspect ratios, such as CNFs, even at nanometer levels of thickness.

In this work, we grew two different morphologies of a SnO₂ layer on CNF. We used two types of ALD equipment: flow-type ALD (static ALD), and fluidized bed reactor-type ALD (dynamic ALD). Static ALD could form a discontinuous SnO₂, while a uniform SnO₂ layer was formed by pre-inserting a layer of Al₂O₃. On the other hand, dynamic ALD formed a uniform SnO₂ layer without pre-insertion of an Al₂O₃ layer. X-ray photoelectron spectroscopy analysis revealed that both Sn⁴⁺ and Sn²⁺ were present in SnO₂ on the CNF deposited by static ALD, probably due to the formation of an interfacial layer between the SnO₂ and CNF. When the dynamic ALD method was used, only Sn⁴⁺ was present in the SnO₂ on CNF. Cyclic voltammetry analysis was performed to characterize the electrochemical properties of the SnO₂-coated CNF as an electrode on a direct methanol fuel cell. It was revealed that the discontinuous SnO₂ on CNF deposited by static ALD showed the highest current efficiency as well as enhanced electrocatalytic stability.

1. Introduction

Carbon nanofilament materials, such as carbon nanofibers (CNFs) and carbon nanotubes (CNTs), are promising active materials for electrodes in various energy devices. They present interesting advantages such as network structure, low cost, and electrical conductivity. CNF has especially good properties as a catalyst support material for direct methanol fuel cells (DMFCs), because it has a low electrical resistance ($\sim 10^{-7}$ to 10^{-5} Ωm), large specific surface area (448 m²/g), and excellent thermal and chemical stability [1]. However, there are two major problems with DMFCs employing CNFs: 1) CO poisoning during methanol electrooxidation [2] and 2) non-uniform Pt dispersion by strong C-C bonding on the CNF surface [3]. CNF has strong C-C bonding, so its surface is very stable, which implies that reactive sites for uniform nucleation are scarce [4]. Stable surface-induced Pt aggregation reduces electrocatalytic activity. To overcome these problems, researchers have investigated Pt-based alloys such as Pt-Cu [5], Pt-Sn [6], and others. Alternatively, SnO₂, one of the most widely used

metal oxide catalysts, can supply oxygen-containing species such as OH, and can perform two functions [7]: it can help remove the CO species at lower potentials [8,9], and it can enhance Pt dispersion on supported catalysts.



Recent studies have shown that nanoscale coating on CNTs or CNFs increases the output and lifespan of energy storage devices owing to the improvement of their mechanical and chemical properties [10]. Among the various coating methods possible, atomic layer deposition (ALD) demonstrates a good coverage irrespective of the shape and size of the object being coated [11,12]. Therefore, it has the advantage of being able to coat particles with a high aspect ratio, such as CNF, even at nanometer levels of thickness. In a previous study, VO_x-coated multi-walled carbon nanotubes (MWCNTs) by ALD were used for a supercapacitor [13]. In addition, SnO₂-coated CNTs were used for a gas

* Corresponding author.

E-mail address: bjchoi@seoultech.ac.kr (B.J. Choi).

<https://doi.org/10.1016/j.ceramint.2018.07.199>

Received 28 June 2018; Received in revised form 20 July 2018; Accepted 22 July 2018

Available online 23 July 2018

0272-8842/ © 2018 Elsevier Ltd and Techna Group S.r.l. All rights reserved.

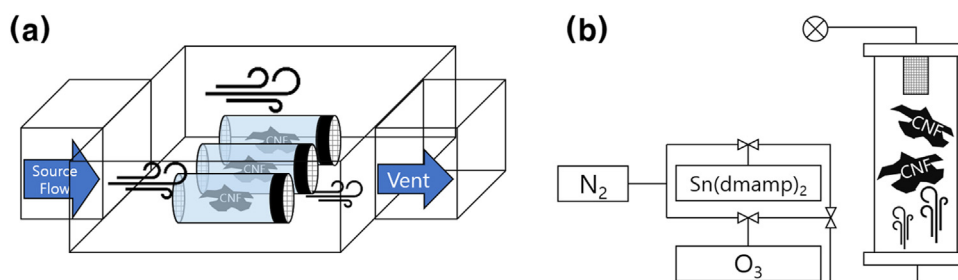


Fig. 1. Schematics of (a) static ALD and (b) dynamic ALD.

sensor [14].

In this study, CNF coated with SnO_2 by ALD is proposed to prevent CO-poisoning and non-uniform Pt dispersion. We can control the morphology of the SnO_2 layer on CNF by ALD [15]. Continuous film and island-type SnO_2 coatings can be formed on CNF by dynamic ALD or static ALD. Pt-coated CNFs with different SnO_2 morphologies were evaluated as a model electrode for DMFCs. The activity of the methanol oxidation reaction was monitored to elucidate the effect of different SnO_2 film morphologies.

2. Experiment

2.1. CNF synthesis

CNFs were synthesized by two steps. First, polyacrylonitrile (PAN, $M_w = 150,000$) nanowires were synthesized by electrospinning. The solution for electrospinning was composed of 10 wt% PAN dissolved in N,N-dimethylformamide (DMF) with stirring for 5 h. For the electrospinning process, the feeding rate of solution was set at 0.03 mL/h. The distance between the collector and the syringe needle was fixed at 15 cm. The voltage and humidity were kept at 13 kV and 10%, respectively, during electrospinning. PAN nanowires were stabilized at 280 °C for 2 h in air and subsequently, carbonized at 800 °C for 2 h under a N_2 (99.999%) atmosphere. The prepared CNFs had a radius of about 240 nm.

2.2. CNF coating

CNFs were coated with SnO_2 by ALD, for which two types of ALD were used. The first is a flow-type ALD (Atomic Classic, CN-1, Korea) with a custom-made container for CNF, and the other is a fluidized bed reactor ALD (iPV d100, ISAC Research, Korea). The flow-type ALD and fluidized bed reactor ALD are denoted hereafter as static ALD (S-ALD) and dynamic ALD (D-ALD), respectively. In S-ALD, the container was constructed with Pyrex glass tubing (SCHOTT, Germany) closed with mesh and an aluminum cap. It was filled with CNFs and placed at the center of the S-ALD chamber.

In S-ALD, SnO_2 was deposited at 161 °C for 105 cycles with tetrakisdimethylamino tin (TDMASn) and H_2O as reactants for a target thickness of 5 nm. One cycle of ALD consisted of 1 s TDMASn feeding - 15 s N_2 purge - 1 s H_2O feeding - 25 s N_2 purge process. To enhance the uniformity of the SnO_2 coating, Al_2O_3 was deposited on CNF at 161 °C for 5 cycles with trimethyl aluminum (TMA) and H_2O as reactants for < 1 nm thickness. One ALD cycle consisted of 1 s TMA feeding - 5 s N_2 purge - 0.5 s H_2O feeding - 25 s N_2 purge process.

In D-ALD, Al_2O_3 was processed at 120 °C for 5 cycles with TMA and H_2O as reactants. SnO_2 was processed at 150 °C for 277 cycles with dimethylamino-2-methyl-2-propoxy-tin(II) ($\text{Sn}(\text{dmamp})_2$) and O_3 as reactants for a 5 nm target. One ALD cycle consisted of 1 s $\text{Sn}(\text{dmamp})_2$ feeding - 5 s purge - 0.5 s O_3 feeding - 25 s purge process.

We prepared four types of samples: SnO_2/CNF and $\text{SnO}_2/\text{Al}_2\text{O}_3/\text{CNF}$ by S-ALD, and SnO_2/CNF and $\text{SnO}_2/\text{Al}_2\text{O}_3/\text{CNF}$ by D-ALD, by using these coating methods.

2.3. Pt dispersion

All the SnO_2 -coated CNF samples were coated with 40 wt% Pt. The CNF samples were dispersed in deionized (DI) water, following which $\text{H}_2\text{PtCl}_6 \cdot x\text{H}_2\text{O}$ (Aldrich) was added to the dispersion. After this process, NaBH_4 (Aldrich) solution was added as a reducing agent. The samples were washed several times with DI water and freeze-dried at - 50 °C using liquid nitrogen.

2.4. Analysis method

Transmission electron microscopy (TEM) (JEM-2100F, JEOL) analysis and energy-dispersive spectroscopy (EDS) mapping data were used for investigating the morphology and chemical composition of the SnO_2 layer on CNF. Surface chemical states were observed by X-ray photoelectron spectroscopy (XPS) (MultiLab2000, ThermoFisher) using non-monochromatic Al K α radiation. Electrochemical characteristics were investigated by a potentiostat/galvanostat (PGST302N, Eco Chemie, Netherlands). A conventional three-electrode system was used, consisting of a working electrode (glassy carbon electrode of area 0.07 cm²), a counter electrode (Pt gauze), and a reference electrode (Ag/AgCl, saturated KCl). The electrolyte was a mixture of 0.5 M H_2SO_4 and 2 M CH_3OH . To measure methanol electrooxidation, all the CNF samples were prepared as mixed inks of 80 wt%-coated CNF and 20 wt % Nafion (Aldrich) in a mixture of 2-propanol (Aldrich) and DI water. Then, the inks of all samples were coated on glassy carbon electrodes. The activity of the methanol electrooxidation reaction was evaluated by cyclic voltammetry (CV) at a scan rate of 50 mV/s in the range of - 0.2–1.0 V. Fig. 1

3. Results and discussion

3.1. Morphology of SnO_2 layer

Morphology analysis and chemical mapping of the SnO_2 -coated CNFs were conducted by TEM-EDS. Fig. 2 shows the TEM images and EDS mapping data of the SnO_2 -coated CNFs. The amorphous SnO_2 layer was darker than CNF in the bright-field image, which was confirmed by EDS mapping.

Fig. 2(a) shows that SnO_2 was sparsely and discontinuously grown on the CNF surface by S-ALD, primarily due to the low reactivity and wettability of the TDMASn precursor and H_2O vapor on the CNF surface. In contrast, a uniform SnO_2 layer was formed by inserting an Al_2O_3 layer on CNF by S-ALD, as shown in Fig. 2(b). The uniform distribution of both Sn and Al were confirmed by EDS mapping. Density functional theory shows that the TMA reaction requires a smaller activation energy than the TDMASn reaction. In the Al_2O_3 ALD reaction, the activation energies of TMA and H_2O are 0.52 eV and 0.7 eV, respectively [14]. In the SnO_2 ALD reaction, the activation energy of TDMASn and H_2O are 1.079 eV and 0.728 eV, respectively [15]. Therefore, the Al_2O_3 layer plays the role of the seed layer for the SnO_2 layer. It has been reported that various methods were used to functionalize its surface to form the uniform ALD film on the substrate

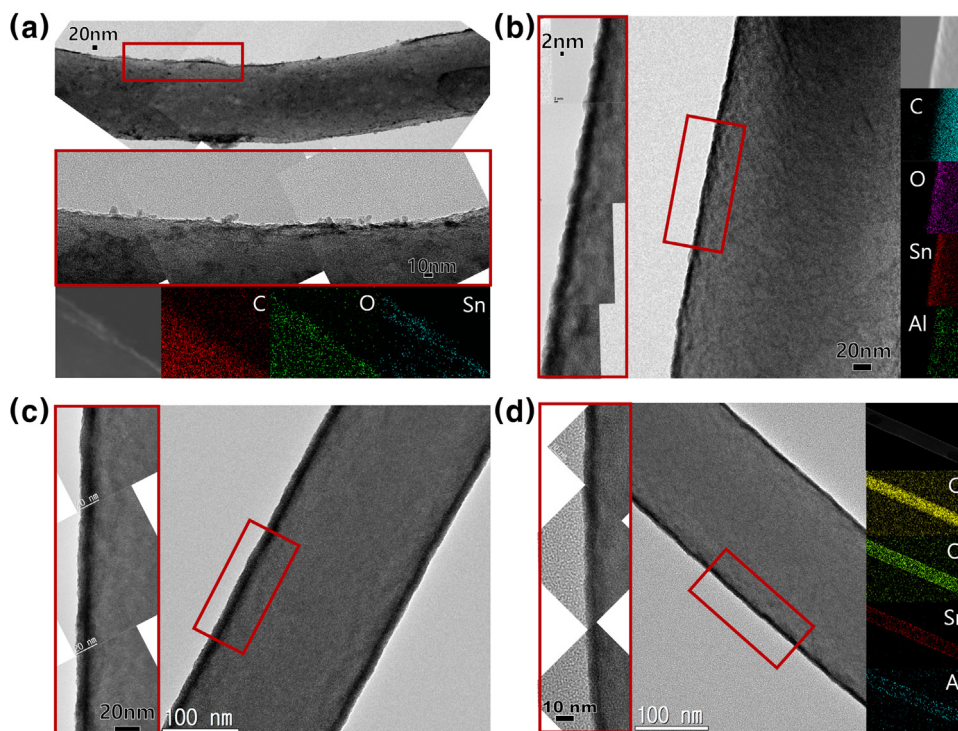


Fig. 2. TEM image and EDS mapping data of SnO₂-coated CNF. (a) S-ALD SnO₂/CNF, (b) S-ALD SnO₂/Al₂O₃/CNF, (c) D-ALD SnO₂/CNF (EDS mapping data not shown), (d) D-ALD SnO₂/Al₂O₃/CNF.

[16–18]; 1) polymer seed layers such as self-assembled monolayers (SAMs), 2) metal or metal-oxide seed layers, 3) the creation of functional groups by plasma or reactive gas functionalization, and 4) wet-chemical treatments such as RCA cleaning or dipping in H₂O.

On the other hand, a uniform SnO₂ layer was formed on CNFs by D-ALD irrespective of the presence of an Al₂O₃ layer, as seen in Fig. 2(c) and (d). In the case of D-ALD, sufficient time and energy for the nucleation could be supplied by agitation of the CNF, although the surface of CNF still lacks a reactive site. In addition to the agitation, O₃ used as reactant for the D-ALD has much stronger tendency to react with the stable surface, which resulted in the generation of reactive site. Therefore, the effect of reactant and mechanical agitation may evoke much lower energy barrier to make uniform layer on CNF surface. This was confirmed by measuring the thickness of the SnO₂ layers.

The thickness frequency of the SnO₂ layers is statistically presented in Fig. 3. The thickness was measured at multiple positions in the TEM images. In the case of S-ALD, 4.2 and 4.8 nm-thick SnO₂ were formed, while D-ALD produced 10.3 and 6.7 nm-thick SnO₂ layers. Insertion of an Al₂O₃ layer led to a thicker SnO₂ layer and a finer thickness distribution in the case of S-ALD. With D-ALD, however, a SnO₂ layer much thicker than expected was formed. The thickness of the SnO₂ layer was in fact diminished by the introduction of an Al₂O₃ layer.

3.2. Surface chemical state

Next, the chemical state of the surface was studied by XPS. For comparison, all the SnO₂-coated CNFs were coated with Pt as mentioned in the experimental procedure.

Fig. 4 shows the XPS spectra of Sn 3d in each sample. There are no metallic Sn peaks observed. However, a significant amount of the Sn²⁺ peak at ~ 486.3 eV [19] as well as Sn⁴⁺ are observed in the CNF coated by S-ALD, as shown in Fig. 4(a) and (b). By deconvolution of the peak, the Sn⁴⁺:Sn²⁺ peak area ratio of SnO₂/CNF was about 1:1, while in SnO₂/Al₂O₃/CNF, this ratio was almost 2:1. It is thought that SnO₂ provides oxygen to the CNF surface when the growth of the SnO₂ layer commences, so that the SnO₂/CNF interface has a SnO phase. When

Al₂O₃ (< 1 nm) was inserted, the amount of the SnO phase can be reduced owing to the formation of Al₂O₃/CNF. In the case of D-ALD, however, CNFs had a thicker SnO₂ layer; therefore, their spectra were close to that of Sn⁴⁺, showing a peak at ~ 487.3 eV [20] in Fig. 4(c) and (d).

Fig. 5 shows the Pt 4f and 4d XPS spectra. Only metallic Pt was observed in the samples at the same energy level. In Fig. 5(a), the peak at ~71.2 eV [21] refers to the binding energy of metallic Pt in 4f_{7/2}. Moreover, Fig. 5(b) shows peaks at ~314.8 eV [22,23], which represent the binding energy of metallic Pt 4d_{5/2}. We used the peak intensity to compare Pt dispersion. Although a thicker SnO₂ layer was formed on CNF by D-ALD, stronger Pt peaks were observed in both Pt 4f and 4d spectra of the CNF coated by S-ALD. Generally, Pt has tendency to aggregate on stable surface. So it demands a nucleation site to make well-dispersed Pt at nanoscale. Metal oxide can play a role of such a nucleation site by providing hydroxyl group. In this point of view, SnO₂ layer coated by static ALD might give more reactive site to Pt, which causes difference of dispersed Pt atom. Therefore, it appears that more Pt was dispersed on the CNF surface coated by S-ALD.

Fig. 6 shows a schematic diagram of morphology and chemical state of the SnO₂ layer, considering the results of TEM-EDS and XPS analysis.

3.3. Electrochemical properties

Cyclic voltammetry (CV) curves of DMFC using SnO₂-coated CNFs were measured by a potentiostat/galvanostat in 0.5 M H₂SO₄ and 2 M CH₃OH electrolytes. DMFC using CNF without a SnO₂ layer showed a forward peak at 0.79 V and a backward peak at 0.61 V as shown in Fig. 7. The SnO₂-coated samples have a forward peak at 0.65 V, and a backward peak at 0.47 V. Both voltage peaks were shifted downwards due to the electrochemical reaction of the SnO₂ layer with the Pt electrocatalyst. The forward peak intensity (I_f) represents the anodic current density corresponding to methanol electrooxidation [24]. The backward peak intensity (I_b) corresponds to the formation of intermediate species of CH₂OH, HCOOH, CO, and CHO. Therefore, the higher I_f related to the anodic current density implies a more efficient

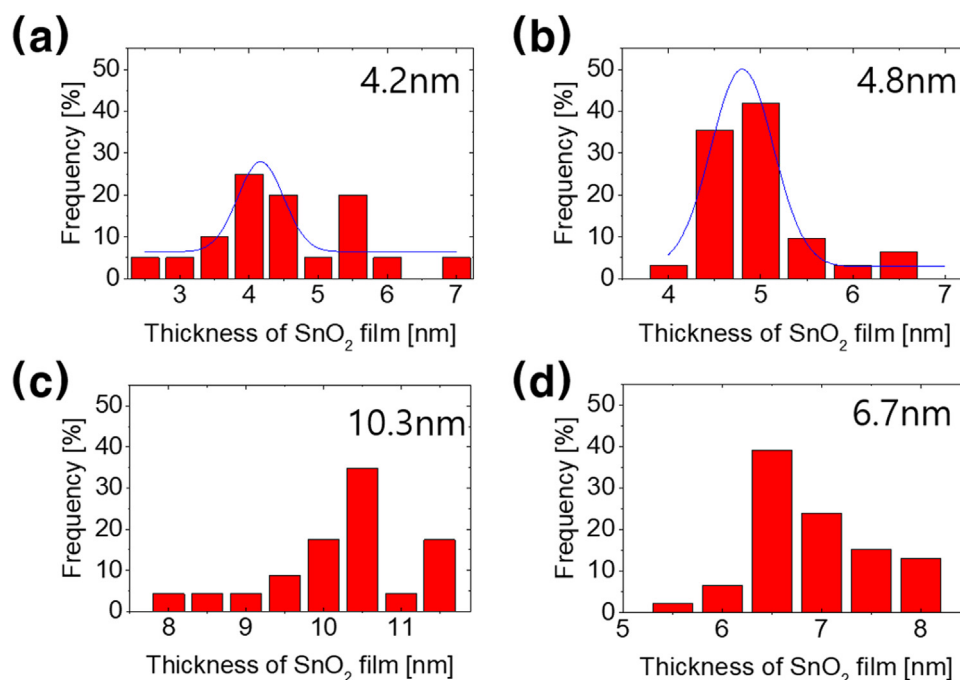


Fig. 3. Thickness distribution of (a) S-ALD SnO₂/CNF, (b) S-ALD SnO₂/Al₂O₃/CNF, (c) D-ALD SnO₂/CNF, (d) D-ALD SnO₂/Al₂O₃/CNF.

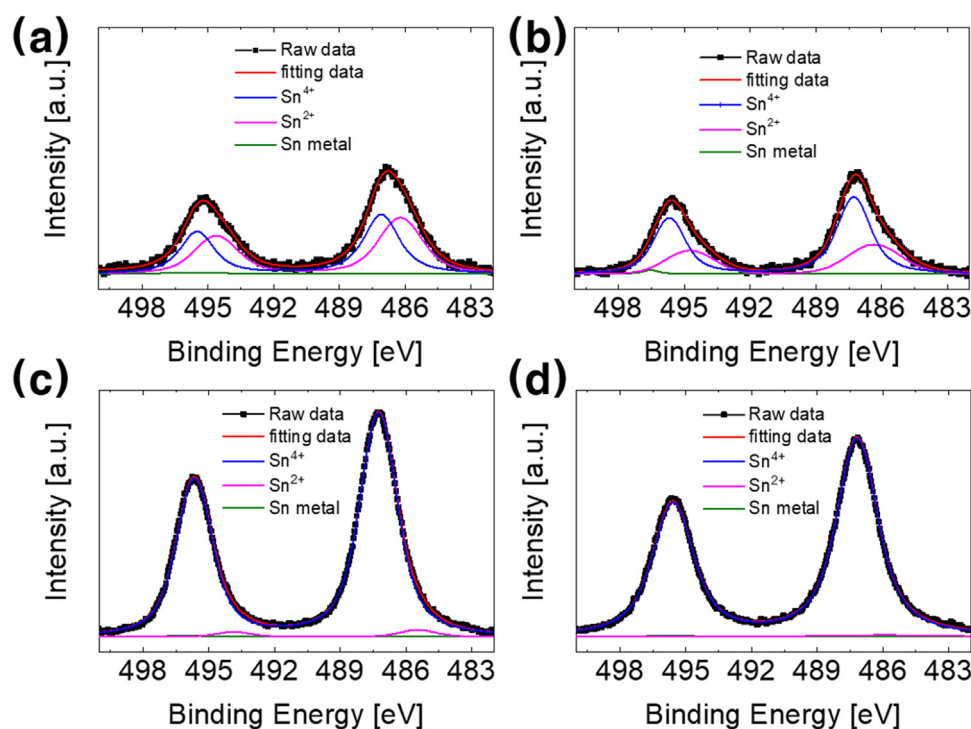


Fig. 4. XPS Sn 3d spectra of SnO₂ layer for (a) S-ALD SnO₂/CNF, (b) S-ALD SnO₂/Al₂O₃/CNF, (c) D-ALD SnO₂/CNF, (d) D-ALD SnO₂/Al₂O₃/CNF.

electrocatalytic activity. I_b can also increase with I_f owing to the formation of intermediate species by the electrocatalytic effect of Pt.

The I_f of the DMFC with CNF as a reference is $508 \text{ mA mg}_{\text{Pt}}^{-1}$. Meanwhile, that of the cell with SnO₂-coated CNF by S-ALD is $575 \text{ mA mg}_{\text{Pt}}^{-1}$. Moreover, the ratio between the current densities of the forward and backward peak (I_f/I_b) of CNF and SnO₂-coated CNF by S-ALD are 0.89 and 1.02, respectively. Such an increase of both I_f and I_f/I_b denotes an enhanced electrocatalytic effect and tolerance of the electrocatalysts to the bi-functional effect of the SnO₂ layer.

In addition to the electrocatalytic effect of the SnO₂ layer, its effect

on electrical conduction should be considered when used as an electrode material for DMFC. When CNFs uniformly SnO₂-coated by S-ALD and D-ALD were used as electrode materials, the anodic current density was significantly reduced, as shown in Fig. 7. Such retardation can be attributed to the electrically relatively resistive SnO₂ layer. A uniform SnO₂ layer sheathes the CNF, so that it can inhibit electrical conduction through the CNF network. The Al₂O₃ layer is more insulating, which makes electrical conduction even more difficult. Therefore, coating with island-shaped SnO₂ can enhance the electrocatalysis of DMFC by helping Pt dispersion and its own bi-functional effect, while electrical

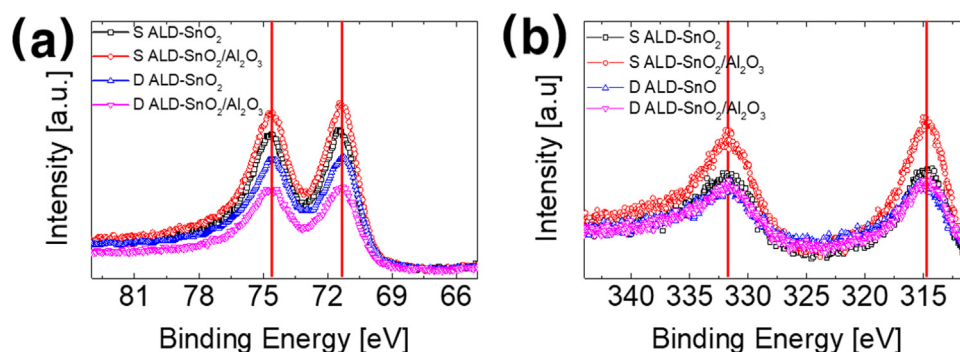


Fig. 5. XPS spectra of Pt-decorated CNF samples. (a) Pt 4f and (b) Pt 4d.

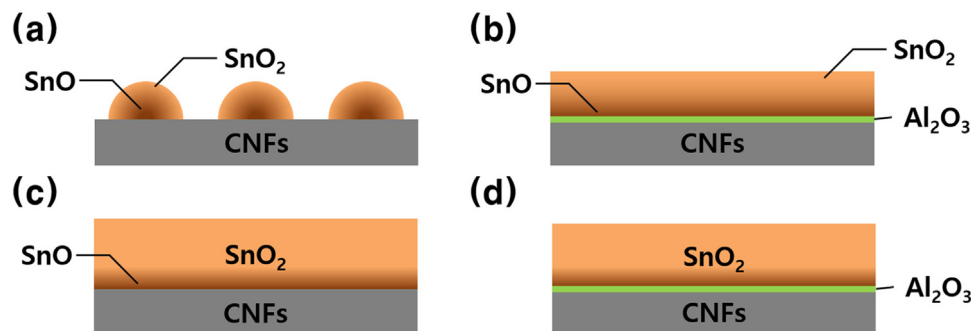


Fig. 6. Schematics of (a) S-ALD SnO₂/CNF, (b) S-ALD SnO₂/Al₂O₃/CNF, (c) D-ALD SnO₂/CNF, (d) D-ALD SnO₂/Al₂O₃/CNF.

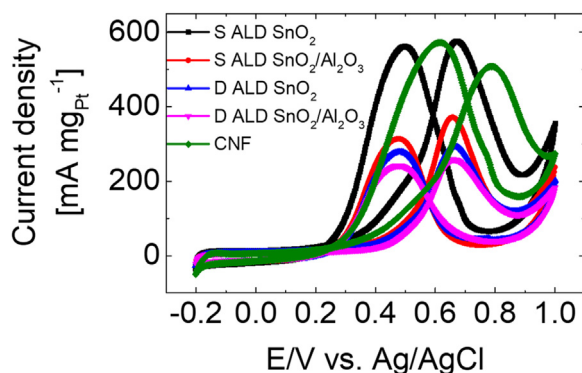


Fig. 7. Cyclic voltammetry curves of methanol oxidation reaction for Pt/S-ALD SnO₂/CNF, Pt/S-ALD SnO₂/Al₂O₃/CNF, Pt/D-ALD SnO₂/CNF, and Pt/D-ALD SnO₂/Al₂O₃/CNF.

conduction is not much affected by its morphology. On the other hand, it is worthy to note that DMFC with CNFs uniformly SnO₂-coated by S-ALD and D-ALD exhibited improved I_f/I_b peak ratio of 1.18 and 1.06, because the continuous SnO₂ layer may contribute the decrease of backward current more efficiently.

4. Conclusion

SnO₂ layers with different morphologies could be grown on CNF by S-ALD and D-ALD with/without an Al₂O₃ seed layer. In the case of S-ALD, island-shaped SnO₂ was formed on CNF, while a continuous SnO₂ layer was formed by pre-inserting an Al₂O₃ layer. In the case of D-ALD, uniform and thick SnO₂ layers were grown on CNF irrespective of the presence of an Al₂O₃ layer. XPS analysis revealed that the chemical states Sn²⁺ and Sn⁴⁺ were observed in the SnO₂ layer on CNF coated by S-ALD, showing that a SnO phase existed in the SnO₂/CNF interface. A higher intensity of Pt spectra on the SnO₂-coated CNF by S-ALD was confirmed by XPS analysis. Cyclic voltammetry curves showed that

island-shaped SnO₂-coated CNF by S-ALD exhibited the best performance for application to DMFCs in terms of current density. It was concluded that the morphology of the SnO₂ layer can affect the catalytic effect and electrical conduction when used as DMFC electrodes. Therefore, further material engineering can be performed using ALD as a coating method to control the morphology and electrical properties.

Acknowledgments

This research was supported by Basic Science Research Program through the National Research Foundation of Korea(NRF) funded by the Ministry of Education [2017R1D1A1A09000809]; Nano-Material Technology Development Program through the National Research Foundation of Korea funded by the Ministry of Science, ICT and Future Planning [2009-0082580].

References

- [1] G.H. An, H.J. Ahn, Activated porous carbon nanofibers using Sn segregation for high-performance electrochemical capacitors, *Carbon* 65 (2013) 87–96.
- [2] Z. Jusys, J. Kaiser, R.J. Behm, Composition and activity of high surface area PtRu catalysts towards adsorbed CO and methanol electrooxidation: a DEMS study, *Electrochim. Acta* 47 (2002) 3693–3706.
- [3] G.H. An, T.K. Lee, H.J. Ahn, Research and application of carbon nanofibers, *J. Korean Powder Metall. Inst.* 22 (2015) 367–375.
- [4] P. Zhang, C. Shao, Z. Zhang, M. Zhang, J. Mu, Y. Liu, In situ assembly of well-dispersed Ag nanoparticles on electrospun carbon nanofibers for catalytic reduction of 4-nitrophenol, *Nanoscale* 3 (2011) 3357–3363.
- [5] F. Saleem, Z. Zhang, B. Xu, X. Xu, P. He, X. Wang, Ultrathin Pt–Cu nanosheets and nanocones, *J. Am. Chem. Soc.* 135 (2013) 18304–18307.
- [6] Y. Ma, H. Wang, S. Ji, V. Linkov, R. Wang, PtSn/C catalysts for ethanol oxidation: the effect of stabilizers on the morphology and particle distribution, *J. Power Sources* 247 (2014) 142–150.
- [7] F. Ye, J. Li, T. Wang, H. Wei, J. Li, X. Wang, Electrocatalytic properties of platinum catalysts prepared by pulse electrodeposition method using SnO₂ as an assisting reagent, *J. Phys. Chem. C* 112 (2008) 12894–12898.
- [8] M. Huang, W. Wu, C. Wu, L. Guan, Pt₂SnCu nanoalloy with surface enrichment of Pt defects and SnO₂ for highly efficient electrooxidation of ethanol, *J. Mater. Chem. A* 3 (2015) 4777–4781.
- [9] K. Waki, K. Matsubara, K. Ke, Y. Yamazaki, Self-Organized Pt / SnO₂ electrocatalysts on multiwalled carbon nanotubes, *Electrochem. Solid-State Lett.* 8 (2005)

- 489–491.
- [10] T. Aaltonen, O. Nilsen, A. Magrasó, H. Fjellvåg, Atomic layer deposition of $\text{Li}_2\text{O}-\text{Al}_2\text{O}_3$ thin films, *Chem. Mater.* 23 (2011) 4669–4675.
- [11] K. Manandhara, J.A. Wollmershauser, J.E. Boercker, B.N. Feigelson, Growth per cycle of alumina atomic layer deposition on nano- and micro-powders, *J. Am. Vac. Sci. Technol. A* 34 (2016) 021519.
- [12] F. Yang, J. Zhu, X. Zou, X. Pang, R. Yang, S. Chen, Y. Fang, T. Shao, X. Luo, L. Zhang, Three-dimensional $\text{TiO}_2/\text{SiO}_2$ composite aerogel films via atomic layer deposition with enhanced H_2S gas sensing performance, *Ceram. Int.* 44 (2018) 1078–1085.
- [13] S. Boukhalifa, K. Evanoff, G. Yushin, Atomic layer deposition of vanadium oxide on carbon nanotubes for high-power supercapacitor electrodes, *Energy Environ. Sci.* 5 (2012) 6872–6879.
- [14] I.H. Kim, J.H. Kim, B.W. Cho, Y.H. Lee, K.B. Kim, Synthesis and electrochemical characterization of vanadium oxide on carbon nanotube film substrate for pseudocapacitor applications, *J. Electrochem. Soc.* 153 (2006) 989–996.
- [15] D.H. Kim, D.H. Riu, B.J. Choi, Formation of uniform SnO_2 coating layer on carbon nanofiber by pretreatment in atomic layer deposition, *J. Korean Powder Metall. Inst.* 25 (2018) 43–47.
- [16] René H.J. Vervuurt, Wilhelmus M.M. (Erwin) Kessels, Ageeth A. Bol, Atomic layer deposition for graphene device integration, *Adv. Mater. Interfaces* 4 (2017) 1700232.
- [17] H. Zhang, D. Chiappe, J. Meersschaut, T. Conard, A. Franquet, T. Nuytten, M. Mannarino, I. Radu, W. Vandervorst, A. Delabie, Nucleation and growth mechanisms of Al_2O_3 atomic layer deposition on synthetic polycrystalline MoS_2 , *J. Chem. Phys.* 146 (2017) 052810.
- [18] Paul C. Lemaire, Mariah King, Gregory N. Parsons, Understanding inherent substrate selectivity during atomic layer deposition: effect of surface preparation, hydroxyl density, and metal oxide composition on nucleation mechanisms during tungsten ALD, *J. Chem. Phys.* 146 (2017) 052811.
- [19] Y. Widjaja, C.B. Musgrave, Quantum chemical study of the mechanism of aluminum oxide atomic layer deposition, *Appl. Phys. Lett.* 80 (2002) 3304–3306.
- [20] J.T. Tanskanen, S.F. Bent, Insights into the surface chemistry of tin oxide atomic layer deposition from quantum chemical calculations, *J. Phys. Chem. C* 117 (2013) 19056–19062.
- [21] J. Chastain, J. F. Moulder, R. C. King, *Handbook of x-ray photoelectron spectroscopy*, Perkin-Elmer Corporation, Minnesota, 1992.
- [22] R.M. Navarro, M.C. Alvarez-Galvan, M.C. Sánchez-Sánchez, F. Rosa, J.L.G. Fierro, Production of hydrogen by oxidative reforming of ethanol over Pt catalysts supported on Al_2O_3 modified with Ce and La, *Appl. Catal. B: Environ.* 55 (2005) 229–241.
- [23] T. Huizinga, H.F.J. van 't Blik, J.C. Vis, R. Prins, XPS investigations of Pt and Rh supported on $\gamma\text{-Al}_2\text{O}_3$ and TiO_2 , *Surf. Sci.* 135 (1983) 580–596.
- [24] J.W. Magee, W.P. Zhou, M.G. White, Promotion of Pt surfaces for ethanol electro-oxidation by the addition of small SnO_2 nanoparticles: activity and mechanism, *Appl. Catal. B: Environ.* 152 (2014) 397–402.